Chapter 9

RRAM Memories with ALD High-K Dielectrics: Electrical Characterization and Analytical Modeling

Helena Castán, Salvador Dueñas, Alberto Sardiña,
Héctor García, Tõnis Arroval, Aile Tamm,
Taivo Jõgiaas, Kaupo Kukli and Jaan Aarik

Additional information is available at the end of the chapter

http://dx.doi.org/10.5772/66666

Abstract

Resistive switching phenomena with adequate repetitiveness on Ta_2O_5-TiO_2-Ta_2O_5 and TiO_2-Ta_2O_5-TiO_2 stacks are reported. In particular, 5–nm-thick TiO_2 films embedding a monolayer of Ta_2O_5 show the best behavior in terms of bipolar cycles loop width, with separate low and high resistive states up to two orders of magnitude. Tantalum oxide layer increases the defect density in titania that becomes less leaky, and thus, resistive switching effects appear. Small signal ac parameters measured at low and medium frequencies, namely capacitance and conductance, also show hysteretic behavior during a whole bipolar switching cycle. This means that the memory state can be read at 0 V, without any power consumption. High-frequency measurements provide information about dipole relaxation frequency values in the dielectric bulk, and this can be connected with resistive switching behavior. Finally, a double tunneling barrier model fits I-V curves at the low-resistance state even at the bias range where reset occurs and a sharp fall takes place.

Keywords: resistive switching, tantalum oxide, titanium oxide, RF impedance, modeling

1. Introduction

Nowadays, resistive random access memories (RRAMs) have been considered as adequate candidates to replace the current nonvolatile memories, because of their good characteristics

in terms of integration density, speed, power dissipation, and endurance [1, 2]. RRAMs modify the resistivity of metal-insulator-metal (MIM) or metal-insulator-semiconductor (MIS) structures. These devices exhibit a resistive switching (RS) behavior, due to the creation after an initial step (electroforming), of one or several nano-conductive filaments that can connect the two electrodes [3]. Filaments can be broken and formed again by means of an external bias; hence, there are two different resistive states, low resistance (LR) and high resistance (HR). The device can remain in one of the two resistive states for a long time. The RS behavior depends on the dielectric material. Also, top and bottom electrodes play an important role. It has been reported that atomic layer deposited (ALD) transition metal oxides, such as HfO_2, ZrO_2, TiO_2, and so on, exhibit RS behavior [4]. Usually, RS is classified into unipolar and bipolar: The first one depends only on the amplitude of the applied voltage, whereas the second one depends also on the polarity of the applied voltage. Three different mechanisms are considered as responsible for the RS phenomena [5, 6]: the conducting bridge random access memories (CBRAM), in which the conductive filament is formed from the atoms of one of the two metallic electrodes; the valence change mechanism that is attributed to the migration of oxygen anions and a subsequent redox reaction; and finally, the thermochemical mechanism that consists of a change of stoichiometry related to the temperature increment. Despite the great amount of work done, the physic mechanisms of RS are not fully understood; therefore, a great deal of research must be still carried out.

This chapter consists of three parts: In the first one, constituting the main body of this work, resistive switching phenomena on Ta_2O_5-TiO_2-based metal-insulator-metal (MIM) structures are reported. Ta_2O_5-TiO_2 films were grown to target thickness of 6 nm. The films were grown either as nanolaminate-like stacks consisting of Ta_2O_5 and TiO_2 constituent layers, each grown to nominal thickness of 2 nm, or 5- to 6–nm-thick TiO_2 films embedding a monolayer of Ta_2O_5 grown using only 1–3 ALD cycles of Ta_2O_5. The stacks were grown in order to increase the defect densities in titania by inserting otherwise more insulating tantalum oxide and examine the possible effect of the controlled, artificial, layering of different metal oxides to the appearance of resistive switching effect. In the second part, some RF impedance measurement results in more standard metal-insulator-semiconductor (MIS) samples (Ni/HfO_2/Si and W/HfO_2/Si) are shown. The response at frequencies up to 3 GHz is analyzed. The most remarkable fact is that both the relaxation frequency in capacitance curves and the conductance maximum position can vary with the bias voltage depending on the top electrode material. Finally, in the third part of this chapter, two analytical models that fit well the current values in the low-resistance state for Ni/HfO_2/Si structures are described. The first one considers a single tunneling barrier, whereas the second one uses the double tunneling barrier model. A comparison between the two models is carried out.

2. Resistive switching on Ta_2O_5-TiO_2-based MIM structures

MIM samples investigated were obtained by depositing the films on 15 nm-RuO_2/10 nm-TiN/Si substrates. Thin solid titanium tantalum oxide films were grown in an in-house built low-pressure flow-type ALD reactor [7] as stacks formed as TiO_2-Ta_2O_5-TiO_2 or Ta_2O_5-TiO_2-Ta_2O_5

http://dx.doi.org/10.5772/66666

triple layers [8] at the substrate temperature of 350°C. Constituent TiO_2 and Ta_2O_5 layers were grown by using $TiCl_4$ [7] and $TaCl_5$ [9], respectively, as metal precursors. In both cases, ozone, O_3, was applied as oxygen precursor. TiO_2 layers were grown using cycle times 2–2–5–5 s, denoting sequence of $TiCl_4$ pulse length—purge time—ozone pulse length—purge time, respectively. For Ta_2O_5, the corresponding cycle times were 3–2–5–5 s. In all cases studied, these process time parameters allowed reliable self-limited ALD-type growth of constituent layers in this reactor, as evaluated by quartz crystal microbalances in real time prior to the growth of stacked layers. For the growth of Ta_2O_5-TiO_2-Ta_2O_5 stacks, 60 × Ta_2O_5 + 50 × TiO_2 + 60 × Ta_2O_5 ALD cycles were applied, denoting the consequent numbers of the constituent oxide growth cycles. Analogously, for the growth of TiO_2-Ta_2O_5-TiO_2 stacks, 50 × TiO_2 + 70 × Ta_2O_5 + 50 × TiO_2 ALD cycles were applied. Additional TiO_2-Ta_2O_5-TiO_2 stacks were also grown after 75 × TiO_2 + 1 × Ta_2O_5 + 75 × TiO_2 and 75 × TiO_2 + 3 × Ta_2O_5 + 75 × TiO_2 ALD cycles. The above-mentioned stacked films will hereafter be denoted as samples (60-50-60), (50-70-50), (75-1-75), and (75-3-75), respectively. Top electrodes were Pt dots with two different areas (0.52×10^{-3} cm^2 and 2.04×10^{-3} cm^2).

$TiCl_4$ was kept at room temperature (22 ± 3°C). $TaCl_5$ was evaporated at 80-85°C from a fused silica boat inside the reactor. O_3 was generated from O_2 (99.999%) in a BMT Messtechnik 802N ozone generator. Ozone concentration measured with BMT Messtechnik 964 analyzer at the reactor inlet was 200–230 g/m^3 at the normal pressure. N_2 (99.999%) was used as the carrier and purging gas. No post-deposition heat treatment was applied on the samples.

The mass thickness and elemental composition of the films were measured by X-ray fluorescence (XRF) spectroscopy method using ZSX400 (Rigaku) spectrometer, recording K_α lines for Ti, Cl, and O, and L_α for Ta. For the calibration of the XRF measurement procedure, binary TiO_2 and Ta_2O_5 films earlier grown to known thicknesses and densities determined by the X-ray reflection (XRR) method were used. Grazing incidence X-ray diffraction (GIXRD) was applied for the examination of the film structure using Smartlab (Rigaku) X-ray diffractometer with CuKα radiation. In accord with the XRF analysis, the (60-50-60) stacks contained 54.5 wt.% Ta, 12.1 wt.% Ti, 32.8 wt.% O, and 0.55 wt.% residual Cl, whereas the (50-70-50) ones contained 48.8 wt.% Ta, 21.0 wt.% Ti, 30.0 wt.% O, and 0.24 wt.% residual Cl. On the other hand, the (75-3-75) stacks contained 10.9 wt.% Ta, 48.7 wt.% Ti, 40.0 wt.% O, and 0.28 wt.% residual Cl, whereas the (75-1-75) ones contained 4.6 wt.% Ta, 53.8 wt.% Ti, 41.4 wt.% O, and 0.23 wt.% residual Cl.

Considering the results of the compositional analysis, the relative amounts of titanium and tantalum (oxides) in the films appreciably correlated with the amounts of cycles applied for either constituent oxide. Certain residual contamination with chlorine was expected due to the presence of chlorine as ligand atoms in both metal precursors and their incomplete removal during surface reactions with ozone. The films deposited to rather low thicknesses of 6 nm and below that were essentially amorphous as revealed by their featureless XRD patterns (**Figure 1**). Short-range order was recognized, however, in the TiO_2-rich films deposited using the cycle sequence 75-1-75, that is, in the film containing markedly less than one monolayer of Ta_2O_5 between two TiO_2 layers both grown using 75 ALD cycles. The amorphicity of the films can be explained taking into account that layers are too thin to become ordered

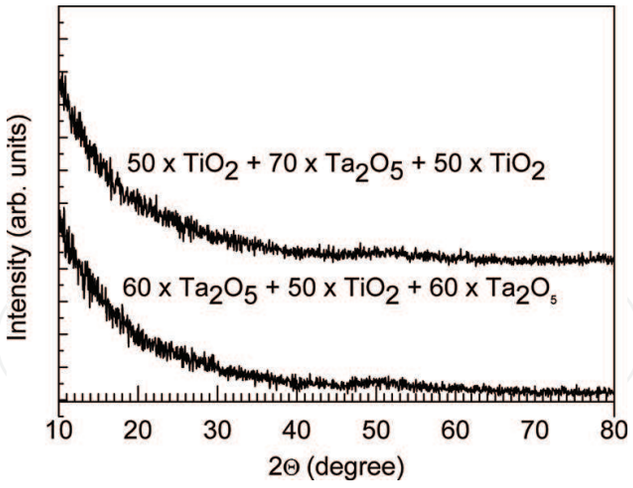

Figure 1. Grazing incidence X-ray diffraction (GIXRD) patterns from nanolaminate TiO_2-Ta_2O_5-TiO_2 and Ta_2O_5-TiO_2-Ta_2O_5 stacks. The numbers of both constituent oxide growth cycles in sequence is indicated by labels.

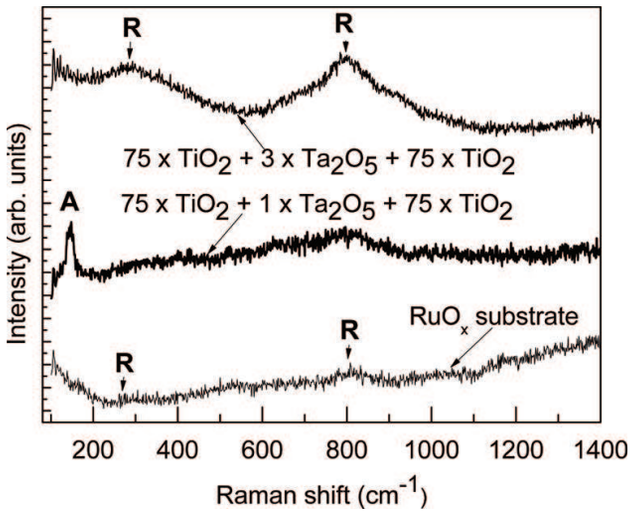

Figure 2. Raman spectra from bare ruthenium oxide electrode (bottom curve), and TiO_2-Ta_2O_5-TiO_2 stacks grown applying one (middle curve) and three (top curve) ALD cycles of Ta_2O_5 between TiO_2 layers. The total film thicknesses were 5.0 and 5.5 nm, respectively.

crystallographically. Moreover, the layers consist of mixed materials foreign to each other both chemically and structurally. This, as any other doping, essentially increases the disorder in the materials, both in terms of long-range and short-range periodicity. In the Raman spectra of the 75-1-75 sample (**Figure 2**), a peak typical for anatase phase was detected at 143–145 cm^{-1} [10, 11] and also seen earlier in TiO_2 films grown by ALD from $TiCl_4$ to H_2O [12]. In the 75-3-75 sample, three Ta_2O_5 growth cycles were applied between the halves of the TiO_2 host layer, and the structural disorder was evidently increased. Consequently, anatase phase could not be recognized any more. Instead, broad Raman bands appeared at 300 and 800 cm^{-1}, which could not be clearly attributed to any known TiO_2 phase. However, the bands follow those obtained from the bare reference RuO_x electrode substrate. RuO_2 [13] is known as the material possessing rutile structure, and the bands in **Figure 2** are thus denoted with R, to guide the

http://dx.doi.org/10.5772/66666

readers eye. In this connection, these 5- to 7-nm-thick films studied are to be characterized as crystallographically very weakly ordered and highly defective.

Electrical measurements of MIM structures were carried out, putting the sample in a light-tight and electrically shielded box. I-V curves were measured using a HP-4155B semiconductor parameter analyzer. C-V and G-V measurement setup was based on a Keithley 4200SCS semiconductor analyzer. After the study of pristine samples, the filaments in MIM devices were electroformed by DC bias sweeping from 0 to 0.7 V with a current compliance of 10 mA. Then, successive I-V cycles showing low-resistance state (LRS) to high-resistance state (HRS) transitions were recorded with current compliance of 100 mA.

Current measurements were carried out by varying the applied voltage in two modes: DC sweep and pulse modes. It is mandatory to carry out measurements using bias pulses, because in the final high-end applications of RRAM, devices are operated in the pulse mode [14]. **Figure 3** shows filament electroforming and the first resistive switching cycles of a Pt/Ta_2O_5-TiO_2-Ta_2O_5/RuO_x MIM sample at room temperature. Voltage bias applied was progressively varied as it is indicated by arrows. After the first forming cycle at 0.7 V, subsequent voltage ramps were applied showing the two different resistance states. Positive voltages produce the high-resistance state to the low-resistance state transition (set). On the back sweep, the low-resistance state is maintained. Using a negative polarity, when voltage reaches the values of about −1 V, the device is switched back to the high-resistance state (reset). Thus, this sample exhibits bipolar resistance switching at low-voltage values. RS parameters are independent on the electrode area; therefore, the switching mechanism is governed by filamentary conduction. The most likely hypothesis is the generation of oxygen vacancies under the applied electric field during positive forming sweep [15]. Oxygen vacancies tend to cluster and generally form filamentary shapes under an electric field. When such clusters are formed, the resistance of the local region becomes much lower than that of the surrounding oxide, and the low-resistance and high-resistance states will therefore be determined by the creation and

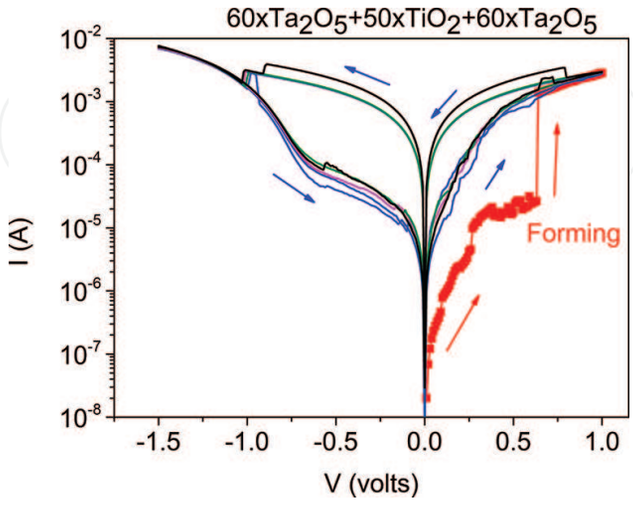

Figure 3. CF electroforming and the first bipolar switching cycles of Pt/Ta_2O_5-TiO_2-Ta_2O_5/RuO_x MIM samples at room temperature.

rupture of the filaments, respectively, which percolate through the sample. In general, set and reset loops are asymmetrical, as it is seen in **Figure 3**. Electroforming in bipolar switching may be a process of introducing asymmetric interfaces in a two-terminal switching cell, which are beyond the asymmetry due to asymmetric electrodes, that is, different top and bottom electrodes. Thus, the electroforming may take one of the two interfaces as an active interface, depending on the polarity of the electroforming voltage, so that reactions taking place in the vicinity of the active interface are responsible for the subsequent bipolar switching [6].

Pulsed biasing comprises positive and negative pulses which lead the samples to the low-resistance and high-resistance states, respectively. To illustrate this technique, we have included the example for a Pt/Ta_2O_5-TiO_2-Ta_2O_5/RuO_x MIM capacitor in **Figure 4**. Using stair-shaped voltage instead of a voltage ramp allows us to record current transients at different states. In this case, we can see that current transients appear when switching to negative voltages, that is, in the reset process (low-resistance to high-resistance transition). Interestingly, resistive switching affects not only the dc currents, but also the small signal ac parameters measured at low and medium frequencies. Indeed, capacitance and conductance also show hysteretic behavior during a whole bipolar switching cycle, as we can see in **Figure 5**. Both magnitudes varied in great extent when the sample was driven from the low-resistance state to the high-resistance state or *vice versa*, even at 0 V bias. This fact indicates that the memory state can be read at 0 V by sensing the admittance at 0 V, without any power consumption.

In order to study the influence of set voltage values on the RS cycles shape, the following experiment was carried out. After the initial electroforming step, some RS cycles under the same condition of current compliance were made in order to stabilize the process. Once repetitive RS curves were obtained, some cycles were recorded by varying the set voltage values regardless of the current compliance values (see **Figure 6**). By increasing the set voltage values, wider loops were obtained. It can be seen that current increases gradually in the

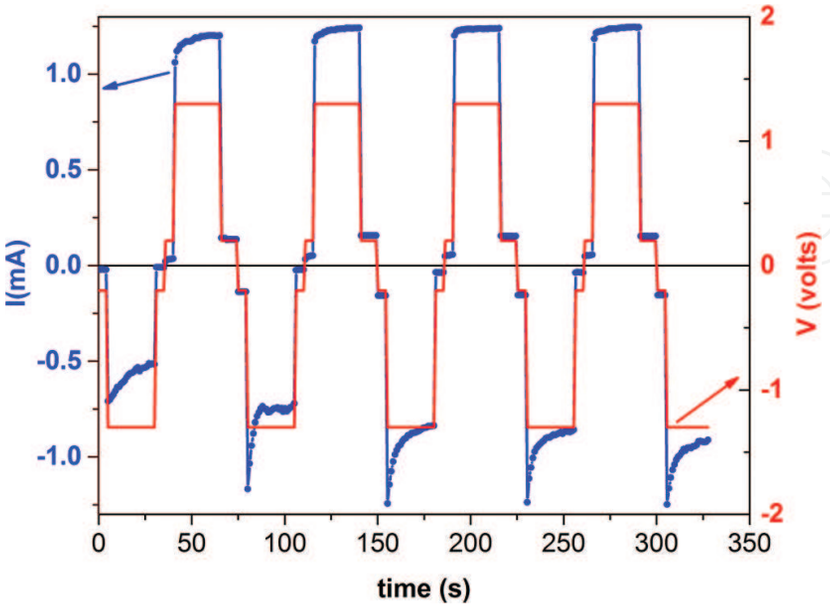

Figure 4. Bipolar switching response to stair-shaped voltage of Pt/Ta_2O_5-TiO_2-Ta_2O_5/RuO_x MIM samples.

http://dx.doi.org/10.5772/66666

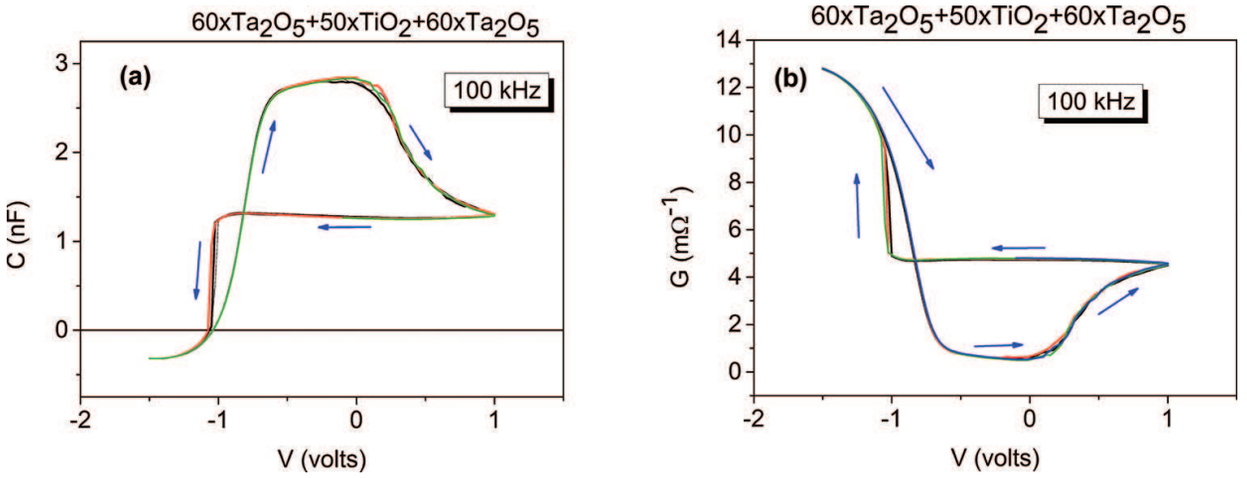

Figure 5. Capacitance (a) and conductance (b) hysteresis during a whole bipolar switching cycle of Pt/Ta_2O_5-TiO_2-Ta_2O_5/RuO_x MIM samples at room temperature.

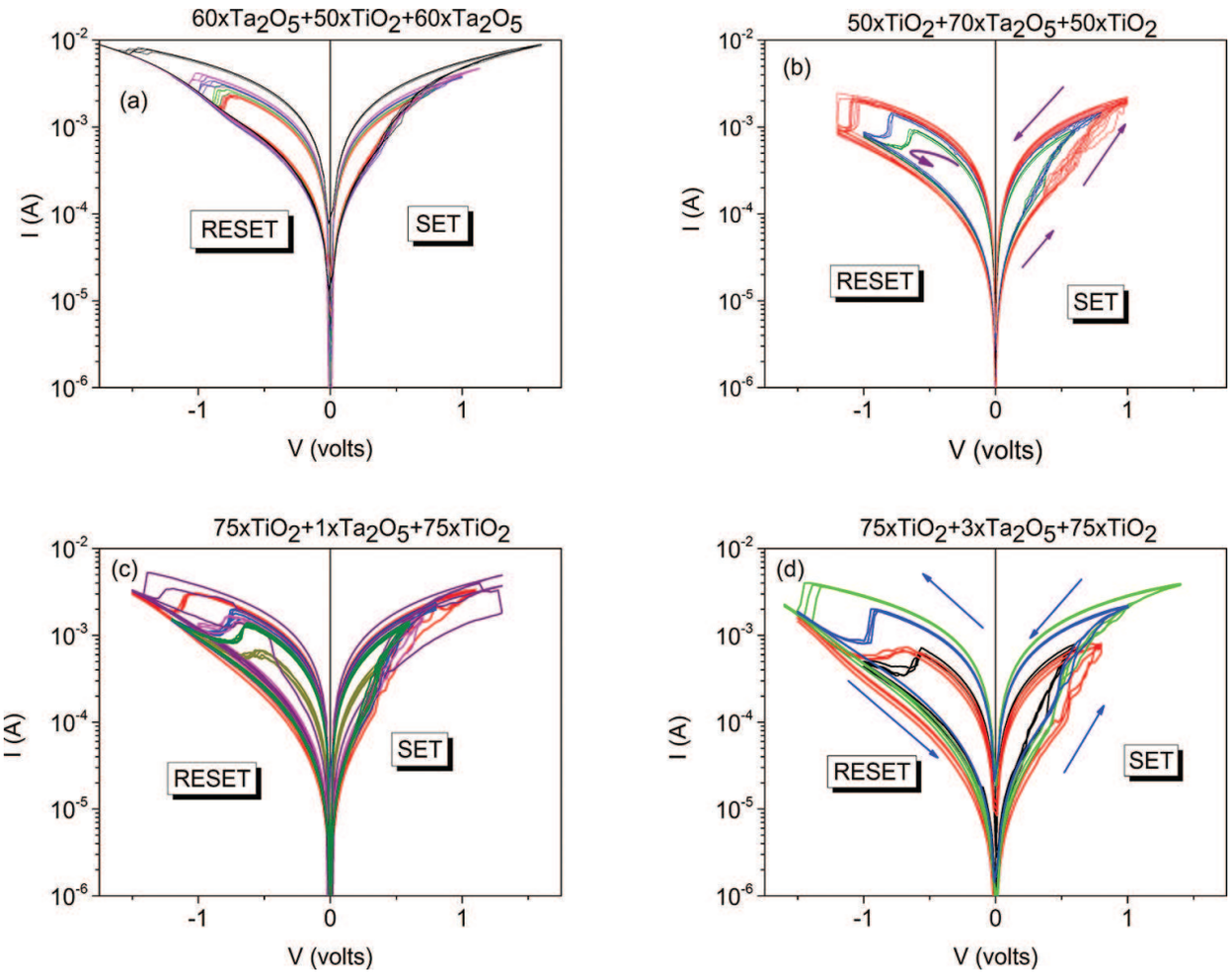

Figure 6. Bipolar switching cycles of Pt/Ta_2O_5-TiO_2-Ta_2O_5/RuO_x and Pt/TiO_2-Ta_2O_5-TiO_2-/RuO_x MIM samples at room temperature, obtained by varying the SET voltage.

set processes, whereas it abruptly falls in the reset processes. From **Figure 6a** and **6b**, it seems apparent that RS cycles are wider in the TiO_2-Ta_2O_5-TiO_2 stacks than in the Ta_2O_5-TiO_2-Ta_2O_5 ones, indicating much more marked differences between high- and low-resistance states when the inner layer is Ta_2O_5. Making very much thinner the Ta_2O_5 layer with respect to the two TiO_2 surrounding layers (**Figure 6c** and **6d**), the RS cycles become wider, but in the (75-1-75) sample, the cycles are not enough stable, providing a mixed picture. On the contrary, the (75-3-75) sample maintains adequate repetitiveness conditions since the very first cycles, and therefore, the two resistive states are clearly distinguished.

In **Figure 7**, the linear correlation between set and reset voltages is depicted for the (75-3-75) sample (blue line). The rise of set voltage values induces a consequent increase in the absolute values of reset voltage. In the same figure, current difference values in the two resistance states measured at a fixed reset value (−0.5 V) for different set voltage values are shown (red line). It is clear that the current window of high- and low-resistance states opens as set voltage value increases. Both tendencies of **Figure 7**, although in minor extent, were also observed in all samples.

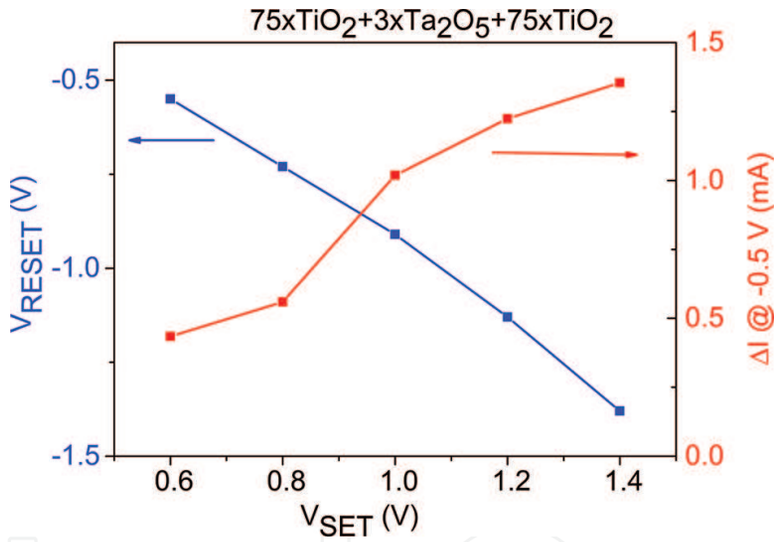

Figure 7. Variation of VReset with VSet of Pt/TiO_2-Ta2O_5-TiO_2-/RuOx MIM samples. The current variation values and VSET relationship are also shown.

3. RF impedance measurements

A deep knowledge of dielectric properties could provide a wider insight of the RRAM behavior. In particular, RF impedance spectroscopy measurements allow detection of the dipolar relaxation of the dielectrics. In a dielectric material, the bound charges are polarized under the influence of an external electric field. Also, surfaces, grain boundaries, and interphase boundaries into the dielectric material contain dipoles that are oriented in an external field and thus contribute to the polarization of the material. When dipole relaxation occurs, the real part of the permittivity, ε′, shows an inflection point, whereas the imaginary part, ε″, has a maximum. In a capacitor, ε′

http://dx.doi.org/10.5772/66666

and ε″ are proportional to the capacitance and conductance signals, respectively. So, admittance measurements at high frequencies provide information about the permittivity relaxation [16].

This study was carried out by using a Keysight E4991B RF Impedance Analyzer, which allowed to carry out measurements in a frequency range of 1 MHz - 3 GHz. Capacitance and conductance of the samples were obtained by scanning the frequency of the ac signal while keeping the gate voltage at a given value. The gate voltage is applied by the voltage source that is built in the E4991B analyzer. A whole RF characterization is obtained by varying the voltage from accumulation to inversion regime. The influence of the gate voltage on the RF characteristics is obtained in this way. In **Figure 8**, we plot RF admittance curves of a W/HfO_2/Si MIS structure. The most noticeable point is the fact that the frequency of the inflection point of the capacitance signal and the maximum of the conductance signal depends on the bias voltage: More positive voltages yield to higher relaxation frequencies. In this case, MIS capacitors are in the inversion regime for positive bias and in accumulation for negative ones. The main conclusion is that the inversion layer at the interface channel affects to the dipole relaxation in such a way that it occurs at higher frequencies. In accumulation, the voltage drop in the oxide is equal to the applied gate voltage, whereas in depletion or inversion regime, part of the applied voltage drops in the semiconductor layer close to the interface. Hence, higher electric field exists on the accumulation regime, dipole orientation is more effective in this regime, and dipoles could not respond to so high frequencies as in the inversion regime. **Figure 9** shows this effect from a three-dimensional point of view.

In order to check the influence of top electrode material on this effect, the same measurements were carried out on similar samples with nickel instead tungsten as top electrode (**Figure 10**). In this case, relaxation occurs at lower frequencies (15 MHz) and no influence of voltage bias on the dipole relaxation frequency values was observed. This can be due to some Fermi level pinning effect in the nickel samples. Also, it can be related to the fact that nickel ions diffuse inside the insulator. These charged ions create local electric fields that interact with insulator dipoles in such a way that relaxation occurs at lower frequencies. Local electric field

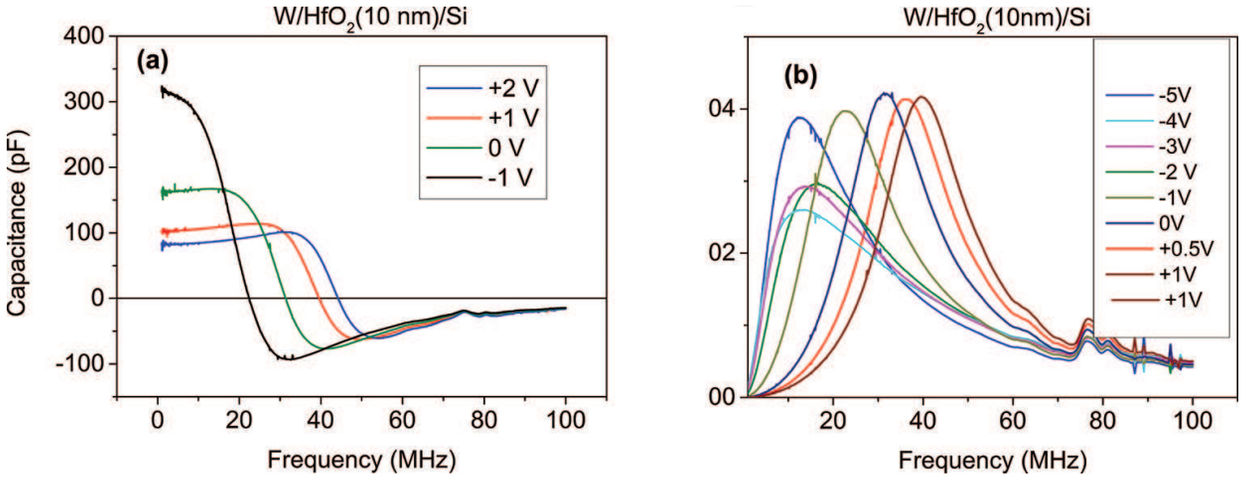

Figure 8. Frequency variations of capacitance (a) and conductance (b) for a W/HfO_2(10 nm)/Si MIS capacitor at different voltage values.

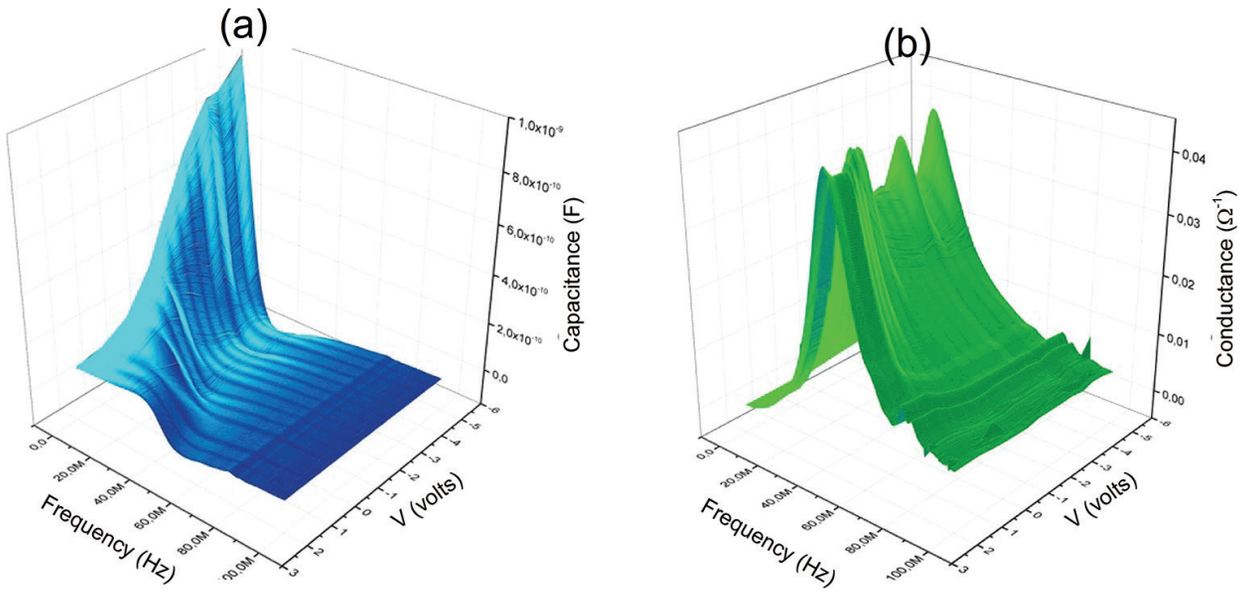

Figure 9. Three-dimensional plots showing frequency and voltage variations of capacitance (a) and conductance (b) for a W/HfO_2(20 nm)/Si MIS capacitor.

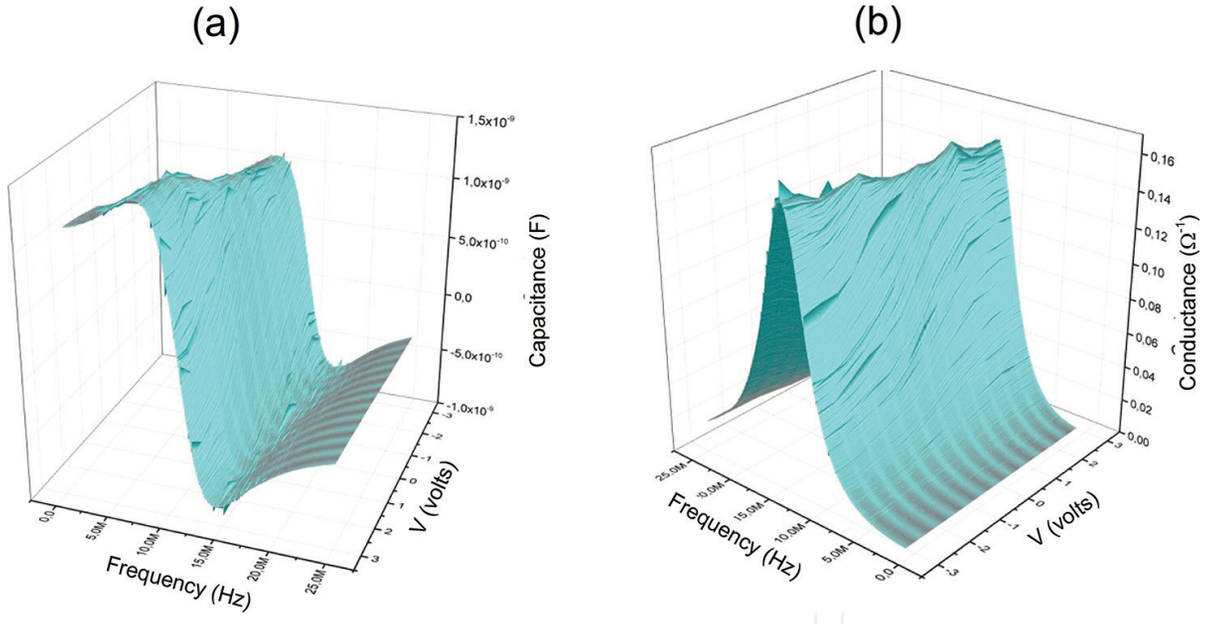

Figure 10. Three-dimensional plots showing frequency and voltage variations of capacitance (a) and conductance (b) for a Ni/HfO_2(20 nm)/Si MIS capacitor.

dominates over the external applied field, and the resonance frequency results independent of the externally applied voltage.

From the resistive switching point of view, it can be worth to point out here that W/HfO_2/Si MIS samples do not show any RS behavior, whereas Ni/HfO_2/Si MIS samples exhibit unipolar RS due to the CBRAM mechanism [8, 17]. The set mechanism is controlled by the thermally

http://dx.doi.org/10.5772/66666

enhanced diffusion of Ni ions induced by local Joule heating, forming a connected nano-filament path. In the reset process, the previously formed filament is partially broken, limiting the current flow. These results agree well with the RF results described before. When no local electric field is detected, there is not resistive switching, as in the W top electrode case. However, in the Ni top electrode case, a local electrical field is detected as a consequence of the diffusion of Ni ions that, in the end, form the conductive filaments thus provoking the RS phenomena.

More detailed studies in this matter should be done in order to connect in more extent the resistive switching behavior with the dielectric properties.

4. Resistive switching modeling

A better knowledge of the nature of the switching behavior requires extending the previous experiments in a wide range of temperatures [18]. We reported an analytical model which fit well with the experimental results for temperatures ranging from 77 to 400 K [17]. This model assumes that the conductive filament does not entirely extend from the top to bottom electrode, and it is interrupted in a region close to one of the electrodes, as is drawn in the inset of **Figure 11**. This gap region behaves as a barrier for the conduction. When the barrier is narrow enough, a current can flow through it by tunneling, and the device is at the low-resistance state. On the contrary, when part of the filament closer to the gap is dissolved, the barrier

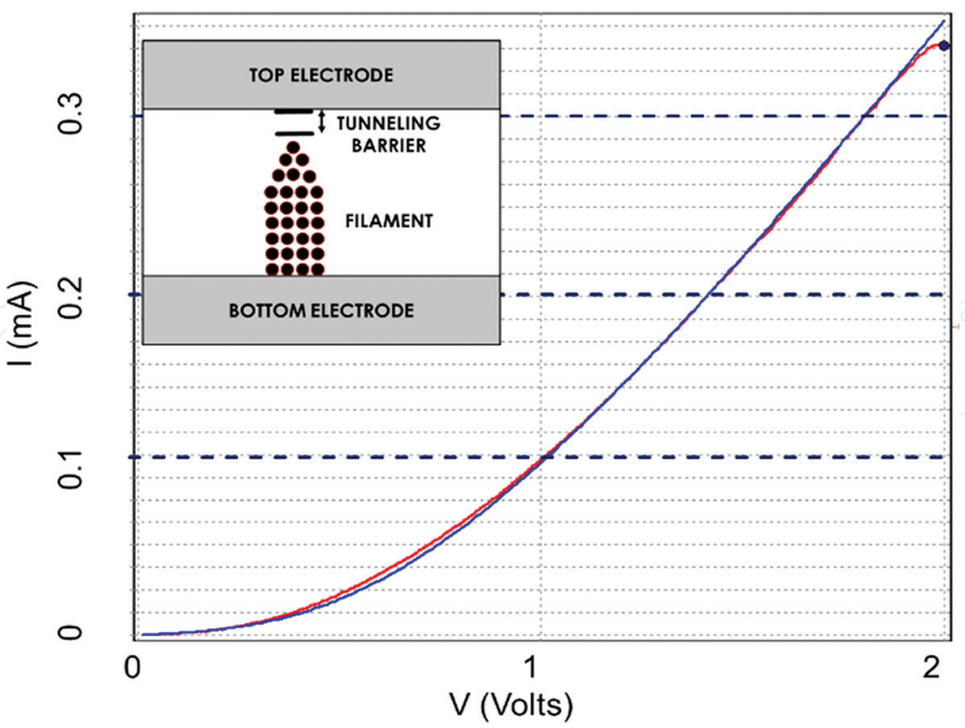

Figure 11. Fitting of a unipolar LRS cycle with the single tunneling barrier analytical model for a Ni/HfO_2/Si MIS capacitor.

becomes thicker and tunneling can-not take place, so producing the low-resistance to high-resistance switching. Very good fitting is obtained with this model as is plotted in **Figure 11**, where the red line is the experimental I-V curves, and the blue line is the best fitting obtained with the following transcendental equation, which is the basis of this model:

$$V_1 = V - \frac{R_\infty}{R_0} \cdot V_1 \cdot e^{\alpha \cdot V_1} \tag{1}$$

where V_1 is the voltage drop in the barrier, V is the applied bias voltage, and $\boldsymbol{R}_0$ and $\boldsymbol{R}_\infty$ are the resistance of the conductive filament at 0 V, and when reset occurs, respectively, α is a parameter very closely related to the barrier tunneling probability, that is, with the filament gap thickness.

An improvement in the previous model assumes a double barrier instead of a single one, as it is illustrated in **Figure 12**. In this model, the current through the barriers is described by a Fowler-Nordheim law as follows:

$$I = \frac{1}{R} \cdot E^2 \cdot e^{-\alpha/E} \tag{2}$$

and the barrier thickness is related to the voltage according a potential law:

$$t(V) = V^\lambda \tag{3}$$

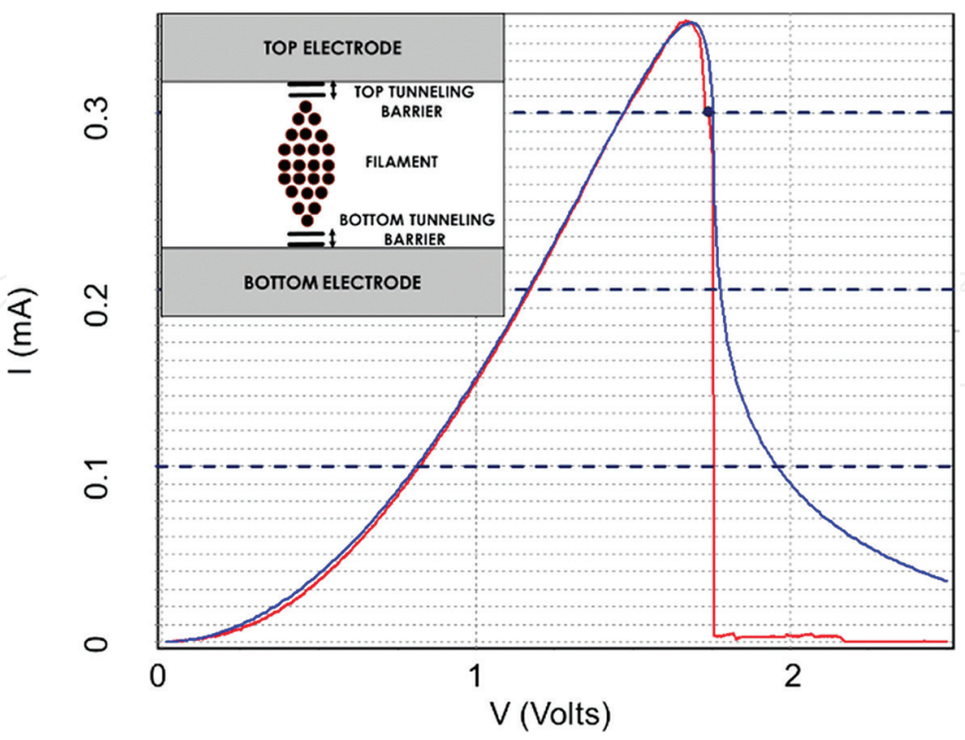

Figure 12. Fitting of a unipolar LRS cycle with the double tunneling barrier analytical model for a Ni/HfO_2/Si MIS capacitor.

http://dx.doi.org/10.5772/66666

5. Conclusions

Resistive switching behavior in Ta_2O_5-TiO_2-Ta_2O_5 and TiO_2-Ta_2O_5-TiO_2 stacks-based MIM structures was reported. Dielectric layers were grown by ALD. The best results were obtained for 75 × TiO_2 + 3 × Ta_2O_5 + 75 × TiO_2 ALD cycles, yielding around 1 monolayer of Ta_2O_5 in a structure with the total thickness of 5 nm. In this sample, wide RS loops were obtained. Moreover, current window of high- and low-resistance states opens as set voltage value increases, with very adequate repetitiveness. In order to try to connect the dielectric properties with the RS behavior, some high-frequency impedance measurements were carried out in W/HfO_2/Si and Ni/HfO_2/Si MIS samples. The detection of a local electric field in the last ones can be related to the diffusion of ions from the top electrode that creates the conductive filament and provoke the resistive switching effect. Finally, an analytical model based on double tunneling barrier was applied to low-resistance cycles of Ni/HfO_2/Si MIS structures, with very good fitting. With respect to the single tunneling barrier, the sharp fall of current at the reset transition (low to high resistance) is also fitted.

Acknowledgements

This work was funded by the Spanish Ministry of Economy and Competitiveness through project TEC2014-52152-C3-3-R, with support of Feder funds, Finnish Centre of Excellence in Atomic Layer Deposition, and Estonian Research Agency (PUT170, IUT2–24), and by the European Regional Development Fund projects TK134 "Emerging orders in quantum and nanomaterials" and TK141 "Advanced materials and high-technology devices for energy recuperation systems". Authors would like to acknowledge Dr. M. B. González and Prof. F. Campabadal (IMB-CNM, Barcelona, Spain) for providing some samples of this study.

Author details

Helena Castán*[1], Salvador Dueñas[1], Alberto Sardiña[1], Héctor García[1], Tõnis Arroval[2], Aile Tamm[2], Taivo Jõgiaas[2], Kaupo Kukli[2,3] and Jaan Aarik[2]

*Address all correspondence to: helena@ele.uva.es

1 Electronic Devices and Materials Characterization Group, Department of Electronics, University of Valladolid, Valladolid, Spain

2 Institute of Physics, University of Tartu, Tartu, Estonia

3 Department of Chemistry, University of Helsinki, Helsinki, Finland

References

[1] Beck A, Bednorz J G, Gerber C, Rossel C, and Widmer D (2000), Appl. Phys. Lett., 77(1): 139.

[2] Waser R and Aono M (2007), Nat. Mater., 6(11): 833.

[3] Kim D C, Seo S, Ahn S E, Suh D S, Lee M J, Park B H, Yoo I K, Baek I G, Kim H J, Yim E K, Lee J E, Park S O, Kim H S, Chung U I, Moon J T, and Ryu B I (2006), Appl. Phys. Lett., 88(20): 202102.

[4] Jeong D S, Thomas R, Katiyar R S, Scott J F, Kohlstedt H, Petraru A, and Hwang C S (2012), Rep. Prog. Phys., 75(7): 076502.

[5] Waser R, Dittmann R, Staikov G, and Szot K (2009) Adv. Mater., 21: 2632.

[6] Lee J S, Lee S, and Noh T W (2015) Appl. Phys. Rev., 2: 031303.

[7] Arroval T, Aarik L, Rammula R, Kruusla V, and Aarik J (2016) Thin Solid Films, 600: 119.

[8] Duenas S, Castán H, García H, Arroval T, Tamm A, Kukli K, and Aarik J (2016) ECS Transact., 72: 153.

[9] Aarik J, Kukli K, Aidla A, and Pung L (1996) Appl. Surf. Sci., 103: 331.

[10] Karunagaran B, Kim K, Mangalaraj D, Yi J, and Velumani S (2005) Solar Energy Mater. Solar Cells, 88: 199, and references therein.

[11] Frank O, Zukalova M, Laskova B, Kürti J, Koltai J, and Kavan L (2012) Phys. Chem. Chem. Phys., 14: 14567.

[12] Tamm A, Acik I O, Arroval T, Kasikov A, Seemen H, Marandi M, Krunks M, Mere A, Kukli K, and Aarik J (2016) Thin Solid Films, 616; 449.

[13] Bhaskar S, Dobal P S, Majumder S B, and Katiyar R S (2001) J. Appl. Phys., 89: 2987.

[14] Niu G, P. Calka P, Maur M A, Santoni F, Guha S, Fraschke M, Hamoumou P, Gautier B, Perez E, Walczyk C, Wenger C, Carlo A D, Alff L, and Schroeder T (2016) Sci. Rep., 6: 25757, doi:10.1038/srep25757.

[15] Hudec B, Paskaleva A, Jancovic P, Dérer J, Fedor J, Rosová A, Dobrocka E, and Fröhlich K (2014) Thin Solid Films, 563:10–14.

[16] Debye P (1929). Polar molecules. Chemical Catalog Company, NY, USA.

[17] Vaca C, González M B, Castán H, García H, Dueñas S, Campabadal F, Miranda E, and Bailón L (2016) IEEE Trans. Electron Dev., 63: 1877.

[18] Fang R, Chen W, Gao L, Yu W, and Yu S (2015) IEEE Electron Dev. Lett., 36: 567.